Threshold Photoionization and Density Functional Theory Studies of the Niobium Carbide Clusters Nb_3C_n ($n = 1-4$) and Nb_4C_n ($n = 1-6$)

Viktoras Dryza, Matthew A. Addicoat, Jason R. Gascooke, Mark. A. Buntine, and Gregory F. Metha*

Department of Chemistry, The University of Adelaide, South Australia 5005, Australia

Received: January 23, 2008; Revised Manuscript Received: March 27, 2008

We have used photoionization efficiency spectroscopy to determine ionization potentials (IP) of the niobium-carbide clusters, Nb_3C_n ($n = 1-4$) and Nb_4C_n ($n = 1-6$). The Nb_3C_2 and Nb_4C_4 clusters exhibit the lowest IPs for the two series, respectively. For clusters containing up to four carbon atoms, excellent agreement is found with relative IPs calculated using density functional theory. The lowest energy isomers are mostly consistent with the development of a $2 \times 2 \times 2$ face-centered cubic structure of Nb_4C_4. However, for Nb_3C_4 a low-lying isomer containing a molecular C_2 unit is assigned to the experimental IP rather than the depleted $2 \times 2 \times 2$ nanocrystal isomer. For Nb_4C_5 and Nb_4C_6, interpretation is less straightforward, but results indicate isomers containing molecular C_2 units are the lowest in energy, suggesting that carbon−carbon bonding is preferred when the number of carbon atoms exceeds the number of metal atoms. A double IP onset is observed for Nb_4C_3, which is attributed to ionization from the both the lowest energy singlet state and a meta-stable triplet state. This work further supports the notion that IPs can be used as a reliable validation for the geometries of metal–carbide clusters calculated by theory.

I. Introduction

Metal−carbide clusters have been shown to possess size-dependent properties,[1,2] like those of bare metal clusters,[3–5] which make them appealing for investigation, as certain species may possess the required balance of properties for applications in nanotechnology. Furthermore, unlike bare metal clusters, metal−carbide clusters possess a mixture of metallic, as well as covalent and ionic, interactions, resulting in different properties that may be useful in various applications.[5] The determination of the structures of small metal−carbide clusters is important in understanding their potential applications and the growth patterns toward larger clusters. In particular, it is important to know at what point during sequential carbon addition do the bonding arrangements change, i.e., when does carbon−carbon bonding become favorable over metal−carbon bonding.

Experiments on niobium carbide clusters in the size range of interest in the present study have been performed by Duncan and co-workers, who found $Nb_4C_4^+$ to be prominent in the photodissociation of larger cationic clusters, indicating enhanced stability for this species.[6] The authors proposed the structure of Nb_4C_4 to be a $2 \times 2 \times 2$ face centered cubic (fcc) structure or nanocrystal. Studies by workers at the Canadian National Research Council have investigated several bare transition metal cluster and transition metal−ligand cluster complexes by pulsed field ionization zero electron kinetic energy (PFI-ZEKE) photoelectron spectroscopy.[5,7] Of interest to the present study, they investigated the species Nb_3C_2, with its ionization potential (IP) determined to be 5.04 eV.[8] The recorded PFI-ZEKE spectrum of Nb_3C_2 displays a relatively long vibronic progression. This spectrum was compared with the simulated PFI-ZEKE spectrum of the lowest energy isomer calculated by DFT, which shows excellent agreement. This isomer has a trigonal bipyramid geometry, with the carbon atoms bound to opposite faces of the triangular niobium cluster. The IP of Nb_4C_4 was also reported (4.43 eV) in this investigation, which was found to be much lower than that proposed by Duncan and Brock from an earlier power dependence study.[9]

IR resonance-enhanced multiphoton ionization (REMPI) spectra have been collected for various niobium carbide clusters by Meijer, von Helden, and co-workers using the FELIX tuneable infrared free electron laser.[10] A single broad absorption resonance was observed for Nb_4C_4 centered at 675 cm^{-1}. The observed resonance is similar to one of two IR-active phonon modes of the metallic NbC (100) surface and is direct evidence for the proposed nanocystalline structure of Nb_4C_4. Furthermore, this discounts a structure which contains carbon−carbon bonding, as this would possess a strong absorbance near 1250 cm^{-1} such as that observed for the Nb_8C_{12} Met–car.[11]

Harris and Dance have carried out a very extensive study on the calculated structures of niobium carbide clusters using density functional theory (DFT).[12] The authors concluded that nanocrystal fragments are favorable for Nb_mC_n clusters where $m > n$, but structures with C_2 units substituting carbon atoms become favorable for $m < n$ (where $m \approx n$).

In this study, we present photoionization efficiency data for niobium carbide clusters, from which accurate ionization potentials are extracted and compared with those calculated by DFT. Particularly, we give evidence for the presence of C_2 units in the Nb_3C_4, Nb_4C_5, and Nb_4C_6 clusters.

II. Experimental and Computational Methods

A. Experimental Methods. The experimental details of the laser ionization experiments are similar to those reported previously.[13] Briefly, the niobium carbide clusters are formed in a supersonic laser ablation source coupled to a time-of-flight mass spectrometer (TOF-MS). A gas mix consisting of 0.02% acetylene seeded in helium is reacted with the ablation products

* To whom correspondence should be addressed. Phone: +61 8 8303 5943. Fax: +61 8 8303 4358. E-mail: greg.metha@adelaide.edu.au.

10.1021/jp800691s CCC: $40.75
Published on Web 06/05/2008

of a niobium rod and is passed along a 15 mm long "condensation tube" before expansion into the first vacuum chamber. The clusters pass through a home-built skimmer into the second chamber that contains a standard Wiley−McLaren TOF-MS arranged perpendicularly with the cluster molecular beam. The neutral clusters are ionized with the frequency-doubled output of a Nd:YAG-pumped dye laser. Because of inefficiencies in the dye laser grating near 425 nm (Wood's anomaly), data points between 210−214 nm are recorded using the first anti-Stokes output from a Raman-shifter operating with H_2. All data points are collected at 0.2 nm intervals. The resultant ions are detected by a double microchannel plate detector, amplified 125× (Stanford SR445) and sent to a digital oscilloscope (LeCroy 9350 AM, 500 MHz) for averaging (1000 laser shots) before being sent to a PC for analysis. Typical laser powers used are 50 μJ/pulse, collimated to a 5 mm diameter beam, as measured using a power meter (Ophir PE10BB). Under these conditions, all ion signals are found to be linearly dependent with laser fluence. During each wavelength (photoionization efficiency, PIE) scan, the laser power is kept constant. To check that long-term intensity fluctuations in the cluster source had not occurred, the laser is returned to the starting wavelength immediately after each scan to ensure that the cluster signal intensity had remained constant.

B. Computational Methods. Geometry optimization and harmonic vibrational frequency calculations were performed using DFT in the Gaussian 03 suite of programs.[14] Initial calculations were performed using the B3P86 method with the SDD basis set to locate a range of geometric isomers for each cluster species at the two lowest spin multiplicities (i.e., singlet and triplet or doublet and quartet) using a range of starting geometries. As a large number of isomers are possible for species containing multiple open-shell transition metals, the starting geometries chosen for optimization were generally based on certain structural motifs; triangular Nb_3 and tetrahedral or butterfly Nb_4 motifs for the metal substructure; carbon atoms were added to Nb_3 "faces" and Nb_2 "edges" (which may generate nanocrystal fragments), and carbon-rich species were explored by replacing C atoms with C_2 and/or C_3 units. As these structural motifs have been shown to be energetically favorable for niobium carbide clusters,[12] we are confident that the global minima have been located. Subsequently, all low-lying isomers (typically within 0.7 eV of a global minimum) were recalculated using the aug-cc-pVTZ basis set on the carbon atoms in an effort to improve the treatment of these atoms, which is herein referred to as the "extended" basis set. For both basis sets, all isomers were initially optimized without any geometry constraint. The minimized isomers were then examined to determine any symmetry properties and the calculations were again repeated within the highest symmetry point group. The symmetry-constrained energy was subsequently compared to the unconstrained energy to ensure that there was no difference. All isomers were characterized with vibrational frequency calculations to determine whether the optimized structure was a true minimum (and provided the data for the predicted IR spectra of Nb_4C_4). All reported isomers, relative energetics, ionization potentials, and molecular symmetries (inc. term symbols) were obtained using the extended basis set. All of the isomers identified using only the SDD basis set are presented in the Supporting Information.

For all the geometries presented herein (and in the Supporting Information), bonds are drawn between niobium atoms if their distance is less than, or equal to, twice the covalent radius (i.e., ≤2.74 Å). Niobium−carbon bonds are drawn at bond lengths

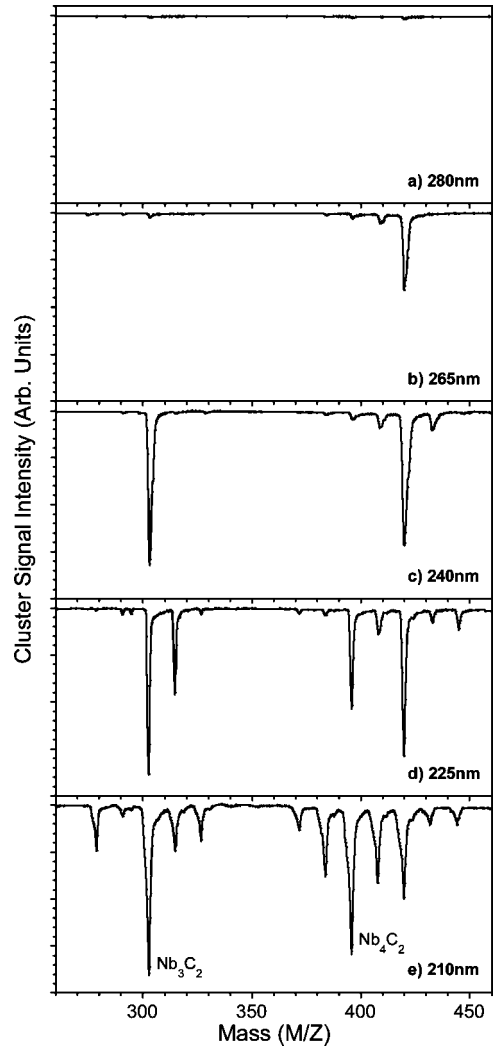

Figure 1. Mass spectra of Nb_3C_n and Nb_4C_n clusters at four different ionization wavelengths: (a) 280, (b) 265, (c) 240, (d) 225, (e) 210 nm.

≤2.35 Å. This distance is longer than the covalent radius of the niobium and carbon atoms combined (2.14 Å) to signify the importance of niobium−carbon bonding and back-bonding effects for isomers with carbon moiety units. Carbon−carbon bonds are drawn as follows: 1.60 Å > single bond > 1.40 Å > double bond > 1.25 Å > triple bond. Atomic charges were determined by natural bond order calculations.[15]

III. Results and Discussion

A. Mass Spectra and Photoionization Measurements. Parts a−e of Figure 1 show a portion of the mass spectrum of niobium carbide clusters following ionization at five different wavelengths; 280, 265, 240, 225, and 210 nm, respectively, under otherwise identical conditions. In the spectrum recorded at 210 nm (Figure 1e), clusters containing Nb_3 appear with 0−4 carbon atoms attached and also clusters containing Nb_4 with 0−6 carbon atoms attached. All of these species are produced following single photonionization.

By contrast to that recorded at 210 nm, the spectrum recorded at 280 nm (Figure 1a) shows that the intensity of all species has decreased dramatically to near baseline levels. At this wavelength, none of the species are ionized with one photon, and the residual signal is due to multiple photon absorption leading to ionization and possibly fragmentation. Although these

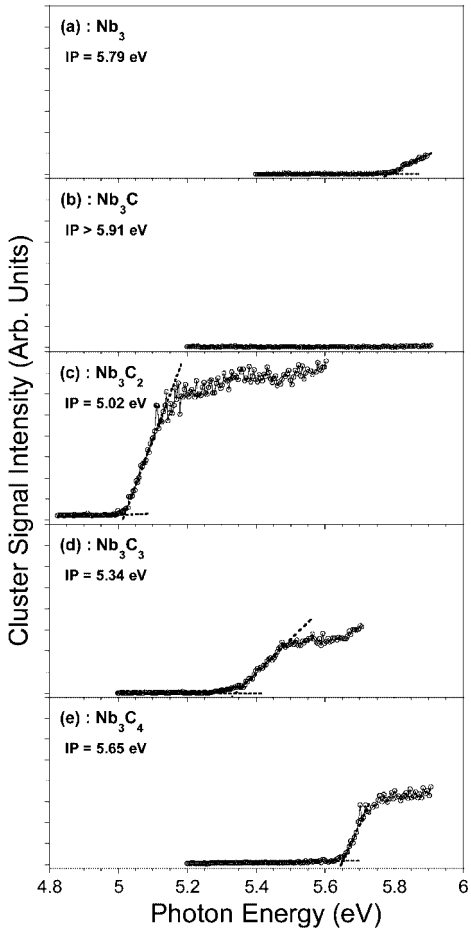

Figure 2. PIE spectra for Nb_3C_n ($n = 0-4$) clusters. The determined IPs are also displayed.

peaks could be diminished completely by lowering the laser power, we found this was not possible without severely affecting the signal-to-noise ratio of the shorter-wavelength spectra. Following ionization at 265 nm (Figure 1b) Nb_4C_4 dramatically increases in intensity, with Nb_4C_3 increasing slightly. At 240 nm (Figure 1c), the clusters Nb_3C_2 and Nb_4C_5 appear. At 225 nm (Figure 1d), the clusters Nb_3C_3, Nb_4C_2, and Nb_4C_6 now appear. Finally back to 210 nm, the clusters Nb_3, Nb_3C_4, Nb_4, and Nb_4C are present, with Nb_4C_3 showing a marked rise in its previous intensity.

PIE spectra were recorded by monitoring the signal of each cluster as a function of wavelength. PIE spectra for the Nb_3C_n ($n = 0-4$) and Nb_4C_n ($n = 0-6$) clusters are shown in parts a−e of Figure 2 and parts a−g of Figure 3, respectively. Nearly all clusters show a dramatic rise from the baseline (e.g., Nb_3C_2 and Nb_3C_4), indicating good Franck−Condon (FC) overlap between the electronic states of the neutral and cation. Many PIE spectra display a leveling off of ion signal quite quickly after the linear rise (e.g., Nb_3C_2 and Nb_3C_3), indicating that the highest-energy FC-allowed transition is quickly attained. However, the clusters Nb_4C_2 and Nb_4C_4 show gradual onsets of ionization containing slight structure, suggesting a significant geometry change between the neutral and cation. Many PIE spectra show ion signal activity just prior to a dramatic rise (e.g., Nb_3C_3). This effect originates from ionization occurring from thermally populated excited levels of the cluster. For all spectra (except Nb_3C, see below) two lines are fitted, one to the baseline and one to the linear rise of signal, and their intersection defined as an appearance potential, which is converted to an IP following the procedure previously described.[13] This method provides a determination of the IP with an estimated error of ±0.05 eV. As a check, the ionization energies extracted for Nb_3, Nb_3C_2, Nb_4, and Nb_4C_4 are found to be in good agreement with those previously determined.[8,16,17]

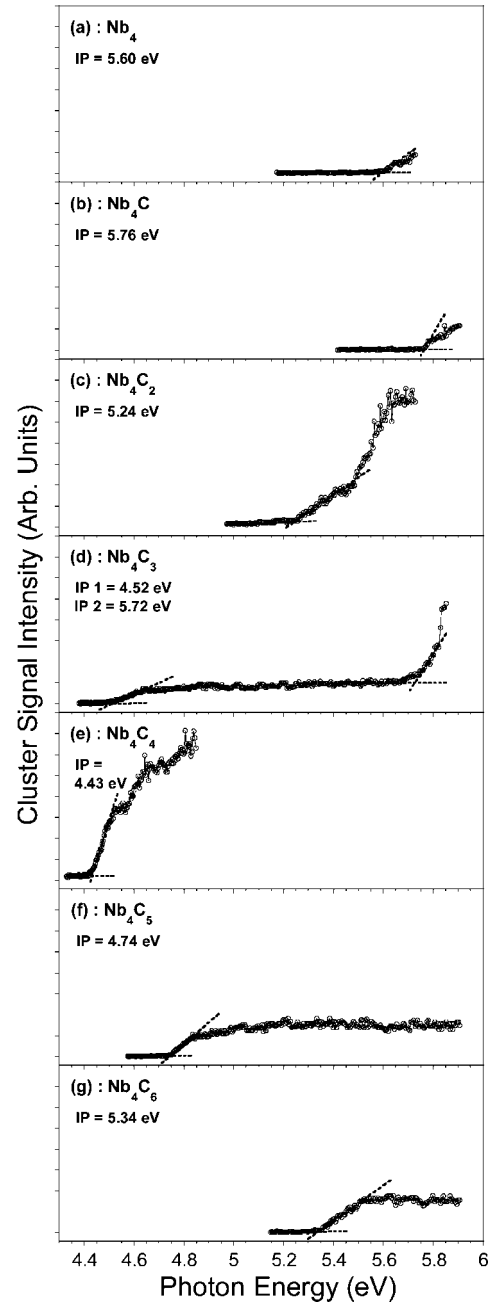

Figure 3. PIE spectra for Nb_4C_n ($n = 0-6$) clusters. The determined IPs are also displayed.

An IP has not been assigned to the cluster Nb_3C, as its PIE spectrum shows no observable onset up to the highest photon energy. We therefore assign the IP of Nb_3C to be greater than the highest achievable photon energy in our laboratory (5.91 eV, 210 nm). The PIE spectrum of Nb_4C_3 displays two separate onsets at 5.72 and 4.52 eV. This will be discussed later, but suffice to say at the moment it is the higher energy onset of greater intensity that we take as the IP. The determined IPs for all the niobium carbide clusters considered in this study are displayed in the PIE spectra and are also given later in the second column of Tables 1 and 2.

Figures 4 and 5 show the determined IPs for each of the Nb_3C_n ($n = 0-4$) and Nb_4C_n ($n = 0-6$) clusters, respectively,

TABLE 1: List of Experimental IPs (Reported in eV) Observed for Nb_3C_n ($n = 0-4$) Clusters (Also Listed Are Calculated Transitions and IPs Excluding Zero Point Energies (ZPE), including ZPE, and offset IP (i.e., IP†))

cluster	exptl IP	isomer	calcd transition	calcd IP (excluding ZPE)	calcd IP (including ZPE)	offset IP
Nb_3	5.79	IA	$^3A_1' \leftarrow {}^2A''$	6.146	6.158	5.790
Nb_3C	>5.91	IIA	$^1A_1 \leftarrow {}^2A_1$	7.072	7.070	6.702
		IIB	$^1A' \leftarrow {}^2A'$	6.116	6.133	5.765
Nb_3C_2	5.02	IIIA	$^1A_1' \leftarrow {}^2A'$	5.560	5.580	5.212
Nb_3C_3	5.34	IVA	$^1A' \leftarrow {}^2A'$	6.071	6.092	5.724
		IVB	$^3A \leftarrow {}^2A$	6.950	6.953	6.585
Nb_3C_4	5.65	VA	$^1A' \leftarrow {}^2A''$	6.727	6.725	6.357
		VB	$^1A \leftarrow {}^2A$	6.094	6.113	5.745

TABLE 2: List of Experimental IPs (Reported in eV) Observed for Nb_4C_n ($n = 0-6$) Clusters (Also Listed Are Calculated Transitions and IPs Excluding ZPE, Including ZPE, and Offset IP (i.e., IP†))

cluster	exptl IP	isomer	calcd transition	calcd IP (excluding ZPE)	calcd IP (including ZPE)	offset IP
Nb_4	5.60	VIA	$^2A_1 \leftarrow {}^1A_1$	5.964	5.959	5.600
Nb_4C	5.76	VIIA	$^2A' \leftarrow {}^1A'$	6.116	6.113	5.754
		VIIB	$^2A'' \leftarrow {}^1A_1$	6.379	6.374	6.015
Nb_4C_2	5.24	VIIIA	$^2B_1 \leftarrow {}^1A_1$	5.856	5.851	5.492
		VIIIB	$^2B_2 \leftarrow {}^1A_1$	6.054	6.050	5.691
Nb_4C_3	5.72	IXA	$^2A_1 \leftarrow {}^1A_1$	6.010	6.010	5.651
	4.52		$^2A_1 \leftarrow {}^3A_1$	5.020	5.045	4.686
Nb_4C_4	4.43	XA	$^2B_1 \leftarrow {}^1A_1$	4.875	4.873	4.514
			$^2B_1 \leftarrow {}^3B$	4.942	4.966	4.607
Nb_4C_5	4.74	XIA	$^2A' \leftarrow {}^1A'$	6.415	6.414	6.055
			$^2A' \leftarrow {}^3A'$	5.361	5.380	5.021
Nb_4C_6	5.34	XIIA	$^2A' \leftarrow {}^1A_1$	6.807	6.809	6.450
			$^2A' \leftarrow {}^3A$	5.892	5.921	5.562
		XIIB	$^2A \leftarrow {}^1A'$	6.926	6.916	6.557
		XIIC	$^2A \leftarrow {}^1A$	6.549	6.551	6.192
		XIID	$^2A \leftarrow {}^1A$	6.577	6.591	6.232
		XIIE	$^2A' \leftarrow {}^1A'$	5.830	5.848	5.489

as a function of the numbers of carbon atoms attached to each cluster. In the Nb_3C_n series, relative to the IP of Nb_3, the greatest reduction is for the addition of two carbon atoms (−0.77 eV), with the reduction decreasing successively with the addition of three (−0.45 eV) and four (−0.14 eV) carbon atoms, respectively. For the Nb_4C_n series, addition of one and three carbon atoms to Nb_4 results in very slight changes in the IP, with slight increases of +0.16 and +0.12 eV, respectively. However, addition of two carbon atoms results in an intermediate IP reduction (−0.36 eV), while addition of four carbon atoms results in a significant IP reduction (−1.17 eV). Addition of five and six carbon atoms results in IP reductions of −0.86 and −0.26 eV, respectively.

B. DFT-Calculated Geometries. All the calculated isomers considered for the *neutral* Nb_3C_n ($n = 0-4$) clusters are shown in Figure 6. Similarly, calculated isomers considered for the *neutral* Nb_4C_n ($n = 0-6$) clusters are shown in Figure 7. The relative energies (eV) for each isomer of the neutral species are also given in Figures 6 and 7. For each isomer, similar geometric minima were also identified on the *cationic* surface; however, these are not included in the figures, but the information appears in the Supporting Information. Almost all discussion herein refers to the neutral systems but reference is made to the cationic systems when results can be compared with previous studies. All details (i.e., geometric and energy information) for both neutral and cationic isomers is contained in the Supporting Information.

1. The Nb_3C_n Cluster Series. The neutral and cationic Nb_3 cluster has been recently investigated at the DFT level with the B3LYP method by the separate groups of Fowler[18] and Balasubramanian.[19,20] Fowler and co-workers reported an obtuse isosceles triangle [$^2B_1$, C_{2v}] and an equilateral triangle [$^3A_1'$, D_{3h}] as the lowest energy structures for Nb_3 and Nb_3^+, respectively. Balasubramanian and co-workers reported the same structure for the neutral but obtain an obtuse triangle for the cation [$^3B_1$, C_{2v}]. These workers also performed multireference calculations on Nb_3 and Nb_3^+ for which they obtain very similar geometries as their DFT calculations, although occasionally a different spin state was found to be the ground state (e.g., the DFT calculation has the ground state of Nb_3^+ as a triplet but the MRCI calculation is a quintet, which cannot be accessed via ionization from the doublet state of the neutral). However, the multireference character of the ground state is significant and highlights that metal clusters, and presumably metal−carbide clusters, contain large amounts of electronic configuration mixing that may be difficult to properly treat via DFT. In our DFT study, we calculate the lowest energy structure of Nb_3, IA [$^2A''$, C_s], to be a scalene triangle. Several isosceles triangular geometries were also tested, resulting in a higher energy minimum and two transition states, for which the imaginary frequencies of the latter lead to the structure of IA. For the cationic state a highly symmetric structure, IA^+ [$^3A_1'$, D_{3h}], was found to be the minimum, in agreement with Fowler.

Two isomers have been found for Nb_3C which differ in the position of the C atom relative to the triangular Nb cluster; one is planar with the C atom bound across a Nb−Nb edge, IIA [$^2A_1$, C_{2v}], and the other has the C atom bound to a Nb face, IIB [$^2A'$, C_s]. The former is found to be lower in energy by 0.317 eV.

Only one isomer of Nb_3C_2 was investigated, IIIA [$^2A'$, C_s], which has the separated C atoms bound on opposite faces of the Nb_3 triangle, in agreement with the previous experimental/theory PFI-ZEKE work.[8] Our calculated electronic state and

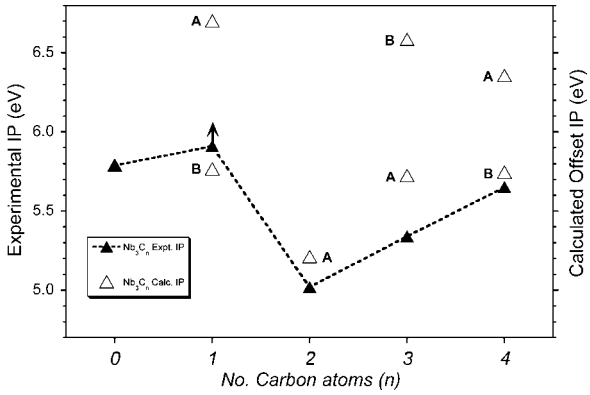

Figure 4. Graph showing experimental values of IP for Nb_3C_n clusters as a function of n. Also shown on the same scale are the offset values, IP†, calculated using DFT. The letters (A, B, etc.) denote the isomers for that particular cluster (see text for details). The upward pointing arrow for the Nb_3C datum represents the experimental IP being a lower bound.

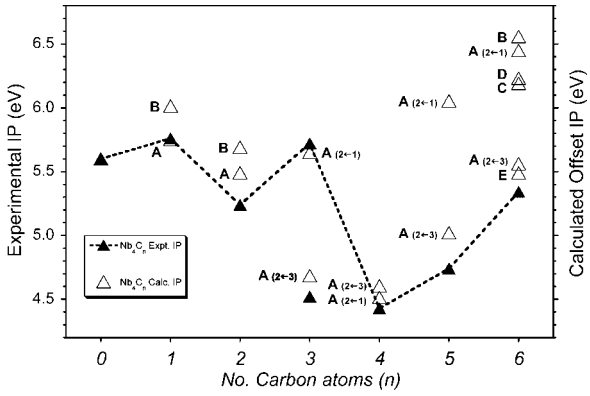

Figure 5. Graph showing experimental values of IP for Nb_4C_n clusters as a function of n. Also shown on the same scale are the offset values, IP†, calculated using DFT. The letters (A, B, etc.) and the numbers (1, 2, etc.) denote the isomers and spin multiplicities, respectively, for that particular cluster (see text for details).

geometry for the cation, IIIA$^+$ [$^1A_1'$, D_{3h}], is also consistent with that study.

The lowest energy isomer of Nb_3C_3, IVA [$^2A'$, C_s], has one C atom bound to a face of the Nb_3 triangle, and the remaining two C atoms are bound across separate Nb−Nb edges, in agreement with that found by Harris and Dance.[12] Isomer IVB [^2A, C_1] has a ΔE of +0.229 eV and contains a C_2 unit bound to a Nb face of the triangular Nb cluster, with the remaining C atom bound across a Nb−Nb edge. Incidentally, the second-lowest energy isomer found by Harris and Dance (at 0.6 eV higher in energy) was found by us to be a transition state (not shown here) leading to IVA.

The lowest energy isomer of Nb_3C_4 is VA [$^2A''$, C_s], which has one C atom bound to a Nb face of the triangular Nb cluster and the remaining three C atoms bound across separate Nb−Nb edges (i.e., a Nb-deficient nanocrystal), in agreement with that found by Harris and Dance.[12] The next lowest energy isomer, VB [^2A, C_1], has a ΔE of +0.183 eV and contains a C_2 unit and a C atom bound to opposite faces of the Nb_3 triangle, with the remaining C atom bound across a Nb−Nb edge. Inspection of the structures in Figure 6 shows that isomer VA can rearrange to become VB by two of its edge-bound C atoms coming together to make a C_2 unit.

2. The Nb_4C_n Cluster Series. As with the niobium trimer, the neutral and cationic Nb_4 cluster has been investigated by the groups of Fowler[18] and Balasubramanian.[19–21] Both groups report an ideal tetrahedral geometry for the neutral [$^1A_1$, T_d], using various computational methodologies. In this study the lowest energy isomer was also found to have ideal tetrahedral symmetry, VIA [$^1A_1$, T_d]. For the cation, Majumdar and Balasubramanian found the lowest energy structure for the B3LYP method to be distorted from the ideal tetrahedral geometry [$^2A'$, C_s]. These workers also investigated Nb_4 at the more accurate multireference level and found there to be significant contributions from several electronic configurations to the ground state.[19–21] Fowler and co-workers also found the lowest energy structure to be distorted [$^2A_1$, C_{2v}]. Similarly, we find the lowest energy structure for the cation to be a C_{2v} structure, VIA$^+$ [$^2A_1$, C_{2v}], with one large, one intermediate, and four small bond lengths. Optimization of Nb_4^+ at the C_s symmetry reported by Majumdar and Balasubramanian was attempted but the geometry and energy was found to be negligibly different from the C_{2v} structure.

Two isomers were found for Nb_4C with the C atom binding either to a Nb face, VIIA [$^1A'$, C_s], or a Nb−Nb edge, VIIB [$^1A_1$, C_{2v}], of the tetrahedral Nb cluster. Isomer VIIA has the lower energy by 0.561 eV.

The structure of the Nb_4C_2 cluster has been previously investigated by the separate groups of Freiser,[22] Dance,[12] and recently Parnis.[23] All groups state that the lowest energy isomer has the two C atoms binding to separate Nb faces of the tetrahedral Nb cluster. We have considered two isomers for Nb_4C_2 and similarly find this to be the lowest energy isomer, VIIIA [$^1A_1$, C_{2v}]. Isomer VIIIB [$^1A_1$, C_{2v}] has both C atoms bound across opposite sides of the open butterfly Nb_4 cluster and is higher in energy by 0.543 eV.

The only isomer of the Nb_4C_3 cluster calculated by Harris and Dance was that of all the C atoms binding to three separate Nb faces of the tetrahedral Nb_4 cluster.[12] We also find the nanocrystal fragment (i.e., a C-deficient nanocrystal) IXA [$^1A_1$, C_{3v}] to be the lowest energy isomer. At the SDD basis set all other isomers were found to be substantially higher in energy (>2 eV).

The results of many experimental and theoretical studies all support the proposal that the lowest energy isomer of Nb_4C_4 has a structure where all four C atoms are bound to all the available Nb faces of the tetrahedral Nb_4 cluster, i.e., two interpenetrating tetrahedra of C_4 and Nb_4 resulting in the formation of a 2 × 2 × 2 cube. Freiser and co-workers were the first to calculate this isomer to support their experimental results.[22] The isomers of Nb_4C_4 have been extensively studied by Harris and Dance, with eight isomers examined and the nanocrystal being significantly the lowest in energy.[12] Consequently, we only explored this isomer and our calculations on the singlet surface yield a highly symmetric structure, XA [$^1A_1$, T_d]. However, we find a triplet state [^3B, C_2] that lies 0.067 eV lower in energy, with its geometry distorted from ideal T_d symmetry.

The Nb_4C_5 species has not been calculated before, although Harris and Dance have proposed for such a species that C_2 units should be energetically favored.[12] We have identified 15 isomers but only 1 is presented here, since all others are >1.8 eV higher in energy at the SDD basis set. This isomer, XIA [$^1A'$, C_s] indeed has a C atom from the 2 × 2 × 2 nanocrystal substituted with a C_2 unit. The structure can also be considered as a C_2 unit bound to the free Nb face of Nb_4C_3 (IXA). From a simple valence bond perspective, structure XIA can be considered as an acetylide (C_2^{2-}) unit undergoing σ interaction with one Nb atom and two side-on π interactions with the other two Nb atoms (i.e., two 3-center 2-electron bonds). A contrasting bonding

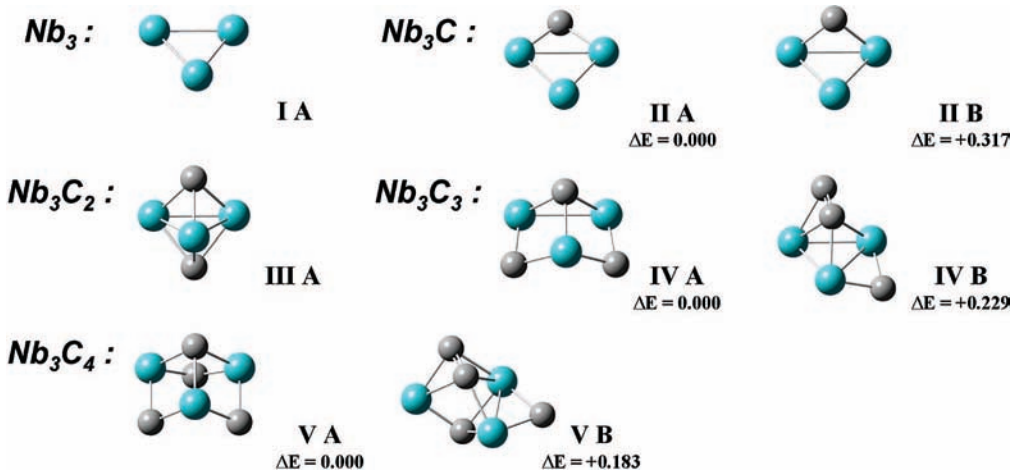

Figure 6. Structures of calculated isomers of neutral Nb_3C_n ($n = 0-4$) clusters. Written beneath each isomer are the relative energies (ΔE in eV) calculated using the extended basis set.

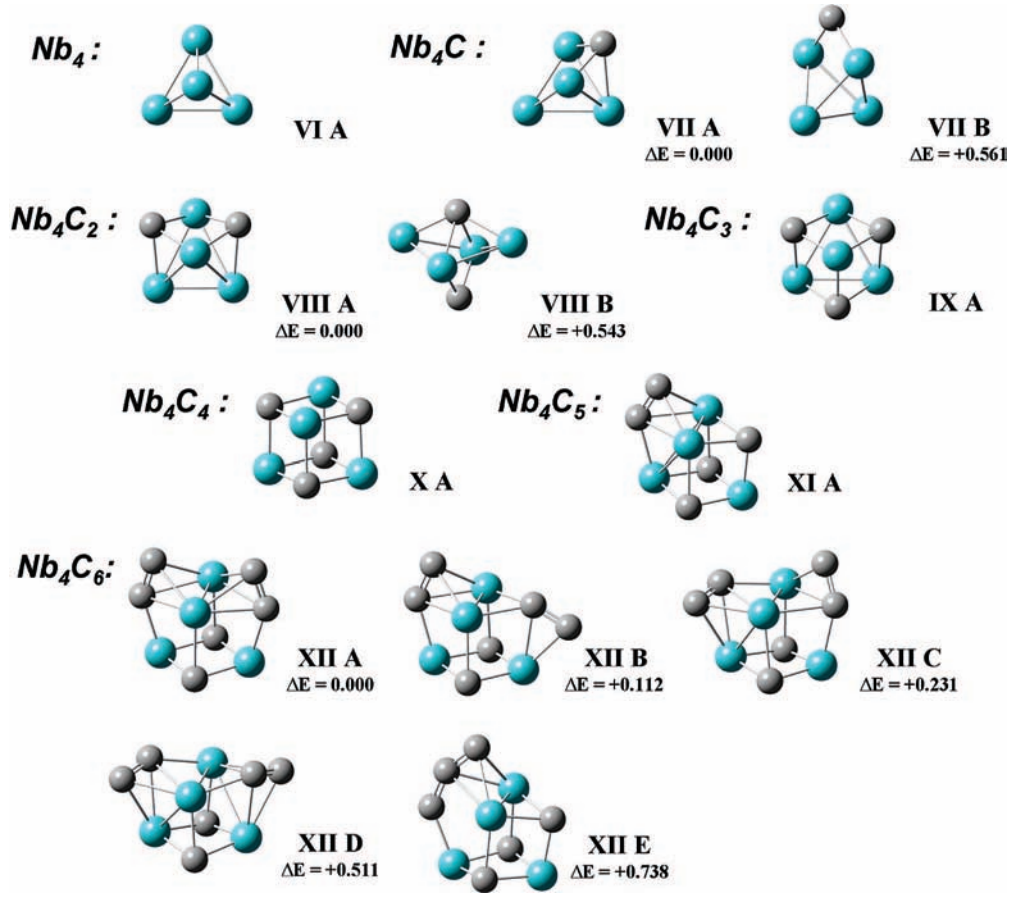

Figure 7. Structures of calculated isomers of neutral Nb_4C_n ($n = 0-6$) clusters. Written beneath each isomer are the relative energies (ΔE in eV) calculated using the extended basis set.

picture can be considered for a C_2 unit having an ethylene (C_2^{4-}) configuration that would form two σ bonds with two Nb atoms and one side-on π interaction with the remaining Nb atom. If the Nb−C bonding in Nb_4C_4 XA is considered as twelve Nb−C 2-center 2-electron bonds, then substitution with a C_2 unit in either configuration could lead to stable electronic structures. However, we find that all starting geometries led to an optimized structure consistent with the former description.

Despite the fact its stoichiometry is exactly half that of the Met–car species, no calculations on Nb_4C_6 have been previously reported. Harris and Dance have proposed (but did not calculate) two isomers for Nb_4C_6, which they found to be key substructures incorporated into larger niobium carbide clusters.[12] These two isomers can be thought of as (unsymmetric) halves of the Met–car structure, each containing three C_2 units. Our calculations using the SDD basis set resulted in 15 isomeric species for Nb_4C_6, with the 2 isomers proposed by Harris and Dance found to be substantially higher in energy (>2 eV). Of the five lowest energy isomers presented here, the four lowest are based around a $2 \times 2 \times 2$ nanocrystal with $2 \times$ C atoms replaced by $2 \times C_2$ units oriented in various ways. The lowest energy isomer, XIIA [$^1A_1$, C_{2v}], has both C_2 units bound in an acetylide configuration, with both units interacting side-on with the same two Nb atoms. By changing one of the C_2 units in XIIA to

have an ethylene configuration gives XIIB [$^1A'$, C_s], which is negligibly higher in energy ($\Delta E = +0.112$ eV). Another isomer related to XIIA is XIIC [^1A, C_1]; where one C_2 unit is rotated ~90°, so that now there is one Nb atom which is σ bonded to one C_2 unit and interacts side-on with the other C_2 unit. XIIC has a ΔE of +0.231 eV. The final isomer of Nb_4C_6 containing two C_2 units is XIID [^1A, C_2], where both C_2 units in XIIA are rotated ~90° toward opposite sides of the cluster, which has a $\Delta E = +0.511$ eV. The next low energy isomer, XIIE [$^1A'$, C_s], can be considered as a C_3 unit substituting one C atom in the $2 \times 2 \times 2$ nanocrystal (i.e., a C_3 unit bound to the free Nb face of Nb_4C_3 IXA). It is 0.738 eV higher in energy than the global minimum.

C. Comparison between Experimental and Calculated IPs. Ionization transitions are considered for the lowest energy isomer, as well as low-lying isomers, for each cluster species. The adiabatic ionization energies are calculated as the difference in energy between the lowest electronic state of the neutral and the lowest electronic state of the cation, *for the same isomer*, which can be accessed following the $\Delta S = \pm 1/2$ selection rule for ionization. These ionization energies are listed for Nb_3C_n ($n = 0-4$) and Nb_4C_n ($n = 0-6$) clusters in Tables 1 and 2, respectively. Note that although ionization energies both excluding and including ZPEs are listed in the tables, only the latter numbers will be considered for discussion. In addition, the calculated IPs for each of the Nb_3C_n ($n = 0-4$) and Nb_4C_n ($n = 0-6$) cluster series, as well as higher energy isomers for some species, are also shown in Figures 4 and 5, respectively.

1. The Nb_3C_n ($n = 0-4$) Cluster Series. It is seen that the absolute calculated IPs for all the Nb_3C_n species are higher than the experimental values. For example, for Nb_3 and Nb_3C_2 (two species which have had their structures and IPs previously determined),[8,16,24] the calculations yield values that are overestimated by 0.368 and 0.560 eV, respectively. Since this study is concerned with the IP following sequential addition of carbon atoms, we only consider the change in IP relative to the bare metal cluster and apply a linear offset to the calculated IP values. For the Nb_3C_n species, an offset of −0.368 eV is applied so that the calculated and experimental IP of Nb_3 coincides. This offset value, hereafter denoted as IP†, is the value shown in the final column of Table 1. Figure 4 shows the experimental value (▲) and calculated IP† (Δ) for each Nb_3C_n cluster species.

As mentioned earlier, we do not believe that the onset for ionization of Nb_3C has been reached and so we mark it as a lower bound at 5.91 eV. In agreement with this observation is the fact that the IP† for Nb_3C IIA is very high (6.702 eV). Another possibility is that isomer IIB, calculated to be only 0.317 eV higher in energy than isomer IIA, is present in our experiment. However, this isomer has an IP† at 5.765 eV, which, if present in significant density in our experiment, should exhibit an ionization onset. Since this is not the case we contend that only isomer IIA is generated in appreciable yield and that photon energies around 6.7 eV (185 nm) are required to ionize it.

The calculated IP† for Nb_3C_2 predicts a lowering of the ionization potential, in agreement with the experimental trend. The IP† for IIIA is only 0.192 eV higher than the experimental IP, providing an estimate of an acceptable deviation between the experimental IP and calculated IP†.

The calculated IP† increases for the lowest energy isomer of Nb_3C_3, IVA, although it is 0.384 eV higher in energy than the experimental IP. The next lowest energy isomer for Nb_3C_3 (IVB) is only 0.229 eV higher in energy; however, the IP† of IVB is 1.245 eV higher than the experimental value. Therefore, we contend that isomer IVA is present in our experiment.

For Nb_3C_4 VA, the predicted IP† is much higher than the experimental IP by 0.707 eV (putting it beyond our experimental photon energy range), which we contend is too large a difference. The next lowest energy isomer, VB, is only 0.183 eV higher in energy than VA and has a much more acceptable deviation between its IP† and the experimental value (+0.095 eV). Furthermore, the cationic geometry of VA is quite different to the neutral state (as shown in Supporting Information, two of the C atoms move significantly), whereas the cationic geometry of VB is similar to the neutral. In terms of FC overlap, isomer VB is expected to give rise to a rapid onset which is what is observed in the PIE curve. Since the energy difference between the isomers VA and VB is smaller than the expected accuracy of the DFT calculations (~0.5 eV), it is possible that (i) VB is in high abundance in the experiment or (ii) it may be the true global minimum. If both VA and VB are present in our experimental conditions then the onset for VA may appear as a second onset at higher energy; however, no evidence of this was observed. Either way, we propose that it is isomer VB that is responsible for the observed ionization onset at 5.65 eV. The assignment of the ionization onset to this isomer is significant in that it contains a molecular C_2 unit, which suggests that carbon−carbon bonding is energetically stable for Nb_3C_n clusters when $n > 3$. This point becomes even more significant in the next section when clusters containing two more carbon atoms than niobium atoms are discussed.

2. The Nb_4C_n ($n = 0-6$) Cluster Series. As observed for the Nb_3C_n series, the absolute calculated IPs for all the Nb_4C_n species are higher than the experimental values. Identical to the procedure for the Nb_3C_n series, a linear offset of −0.359 eV is applied to the Nb_4C_n species (i.e., the calculated and experimental IPs of Nb_4 overlap) and the resultant IP† is the value shown in final column of Table 2. Figure 5 shows the calculated IP† of the isomers (Δ) for each Nb_4C_n cluster species, as well as the experimental IP (▲).

For Nb_4C the experimental IP and calculated IP† for VIIA are essentially identical, with the deviation being −0.006 eV. The IP† of VIIB is also within an acceptable range of the experimental value (+0.255 eV). However, as the IP† of VIIA is in much better agreement and is the lowest energy isomer by 0.561 eV, we assign the observed experimental IP to VIIA.

For Nb_4C_2 the deviation between the experimental IP and calculated IP†s for VIIIA and VIIIB are +0.252 and +0.451 eV, respectively. Isomer VIIIA is calculated to be 0.543 eV lower in energy than VIIIB, and so we have assigned the experimental IP to the former.

For Nb_4C_3 the IP† of the lowest energy isomer IXA is in excellent agreement with the dominant (second) ionization onset at 5.72 eV, with a deviation of only −0.069 eV. Therefore, this experimental IP is assigned to this isomer. The origin of the first, low intensity, ionization onset at 4.52 eV is not obvious. Fragmentation of larger clusters is ruled out on the basis of the high calculated binding energies of Nb_mC_n clusters[12] and the low photon fluences employed in this study. All other isomers are calculated to be much higher in energy (>2 eV), discounting that the initial onset is due to a low-lying isomer. However, we have calculated a triplet state, $^3A_1$, for IXA that is 0.990 eV higher in energy. This state may be meta-stable and could access the same cationic $^2A_1$ electronic state with an IP† of 4.686 eV, a deviation of only +0.166 eV from the weak ionization onset. Therefore, we propose that the two experimental onsets observed for Nb_4C_3 are due to ionization from both a meta-stable $^3A_1$ state and the lowest energy $^1A_1$ state of Nb_4C_3 IXA.

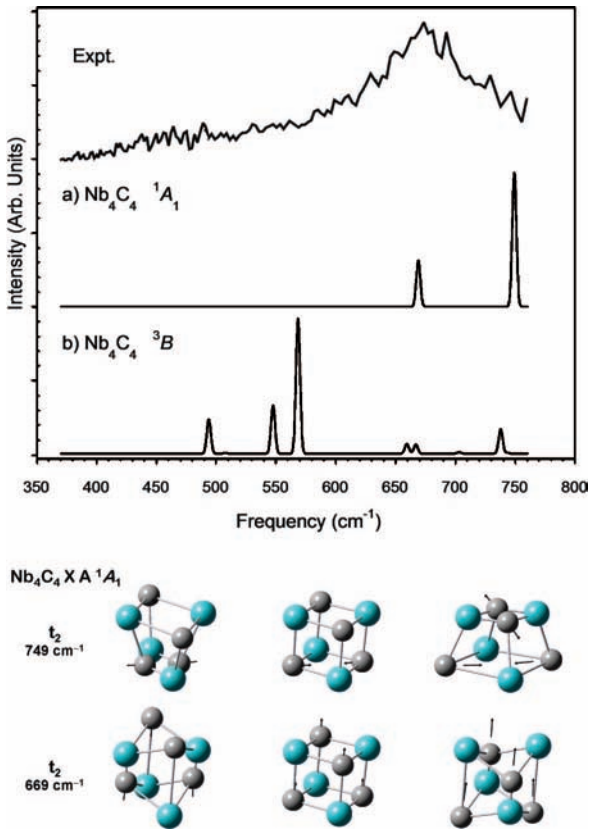

Figure 8. Calculated IR spectra (fwhm = 4 cm^{-1}) for Nb_4C_4 in the $^1A_1$ (trace a) and ^3B (trace b) electronic states. The upper spectrum shows the IR-REMPI spectrum reproduced with permission from ref 10. Also shown are the two t_2 IR-active vibrational modes (one component only) calculated for the singlet state where each mode is represented by the equilibrium position and two extrema.

The only isomer presented for Nb_4C_4 is XA, for which singlet $^1A_1$ and triplet ^3B electronic states are calculated to be separated by only 0.067 eV; the latter being lower in energy. Since the cation is a doublet state, the ionization transition from either the singlet or triplet state could access this cationic state, with both deviations between the experimental IP and calculated $IP^\dagger$ being reasonable (+0.084 and +0.177 eV, respectively). On this basis alone, it is impossible to definitively assign the onset to either spin state.

The IR-REMPI spectrum of Nb_4C_4 has been recorded using an IR free electron laser,[10] and it may be possible to determine if one multiplicity state is preferred experimentally by re-examining its features in combination with our data. The experimental spectrum displays a single broad vibrational absorption band centered at 675 cm^{-1} and the spectrum was analyzed by correlation with one of the two electron energy loss spectroscopy bands of the fcc (100) niobium carbide surface,[25] which supported the notion of the cubic 2 × 2 × 2 structure of Nb_4C_4. Although spectra obtained in single photon IR absorption experiments are not identical to those obtained in IR-REMPI experiments (i.e., intensities can be different), they have been shown to be similar.[11] Figure 8 shows our DFT-calculated IR spectra from the two states of interest (between 370 and 760 cm^{-1} with no scaling, where the IR-REMPI spectrum was recorded). It is readily seen that two vastly different spectra are predicted. Because of its high symmetry, the $^1A_1$ state only exhibits two features, both above 650 cm^{-1}, which are the IR-active triply degenerate modes (t_2 in T_d) corresponding to in-phase and out-of-phase Nb−C vibrations. The motion of the atoms in one component of these two modes is shown in Figure 8. Although only one absorption band was observed in the experimental IR-REMPI spectrum, its breadth almost completely encompasses both of the calculated absorption bands. In contrast, the ^3B state exhibits many more intense features (both *a* and *b* modes in C_2 symmetry), particularly below 600 cm^{-1}, where there are no features in the experimental spectrum. Therefore, given the postulate that the conditions of generating metal-carbide clusters is similar between the two experiments (i.e., ref 10 and this study), we contend that the Nb_4C_4 cluster exists in the singlet state and is the state from which the ionization transition is assigned.

Only one isomer of Nb_4C_5 (XIA) was calculated at the extended basis set, as all other isomers calculated with the SDD basis set were significantly higher in energy (>1.8 eV). The $IP^\dagger$ for XIA is much higher than the experimental IP, with a deviation of +1.315 eV. Furthermore, the $IP^\dagger$ indicates that, similar to Nb_3C, the experimental IP of XIA will be higher than our ionization limit (i.e.>5.91 eV), so even if the isomer were present under our experimental conditions an IP onset would not be observed. One possible explanation for this onset is similar to that of the initial (weak) ionization onset of Nb_4C_3 IXA, that ionization occurs from the (meta-stable) $^3A'$ electronic state of XIA rather than the $^1A'$ electronic state. Since this state is 1.054 eV higher in energy than the singlet state, the calculated $IP^\dagger$ for the ionization transition is 0.281 eV higher than the experimental IP, a much more acceptable deviation (see Figure 5). One point in favor of such an assignment is the appearance of the PIE curve, which is weak and flat, similar to that seen for Nb_4C_3. A firmer assignment could be made if a second, stronger onset was observed, but as discussed above, we expect this to be beyond the photon range of our experiment. Although only a tentative assignment, this is again significant because isomer IXA contains a molecular C_2 unit, which supports the preference for carbon−carbon bonding in Nb_4C_n clusters when $n > 4$.

Five isomers of Nb_4C_6 were examined at the extended basis set, with four isomers (XIIA, XIIB, XIIC, and XIID) containing 2 × C_2 units which only differ in their geometry by the orientation and/or bonding of these two units. The $IP^\dagger$ for XIIA has a deviation of +1.110 eV, relative to the experimental IP, and isomers XIIB, XIIC, and XIID also have large deviations of +1.217, +0.852, and +0.892 eV, respectively (see Figure 5). We consider these deviations to be too large to assign to the observed ionization onset. Furthermore, the predicted $IP^\dagger$s for all four isomers are greater than our highest achievable photon energy. The remaining isomer, XIIE with a C_3 unit, has quite good agreement between the experimental IP and calculated $IP^\dagger$ (+0.149 eV). However, this isomer is calculated to lie significantly higher in energy than XIIA (+0.738 eV) and so could not be reasonably expected to be present in the experiment. Another possibility for assigning the observed ionization onset is a meta-stable excited state, similar to that proposed for Nb_4C_5. The XIA isomer has a ^3A electronic state lying 0.914 eV higher than the $^1A_1$ state. Excitation from this state, to the cationic doublet state, gives an $IP^\dagger$ only 0.222 eV higher than experiment. The appearance of a weak and flat PIE curve, like that observed for Nb_4C_3 and Nb_4C_5, is again consistent with the onset originating from a low abundance state such as a meta-stable electronic state. Clearly it is difficult to separate these two possibilities, which leads to the conclusions that Nb_4C_6 either contains 2 × molecular C_2 units or a C_3 unit; however due to similarity with the Nb_4C_5 system we prefer the former tentative assignment. Finally, we suggest that experiments such as IR-REMPI or IR-multiphoton dissociation (IR-

MPD) could clearly be able to distinguish between these two structural isomers.

Related to the isomers of Nb_4C_6 are several computational studies on the neutral Ti_4C_8 cluster by Wang and co-workers,[26] Sun and co-workers,[27] and Poblet and co-workers.[28] The isomers proposed by Wang and Sun are based on a $2 \times 2 \times 2$ nanocrystal with all the carbon atoms substituted with C_2 units, although they differ in their bonding arrangement; the former structure has all the C_2 units bound in an ethylene configuration and the latter has all the C_2 units bound in an acetylide configuration. The later Poblet study compared these two isomers and found the acetylide isomer to be ~1.4 eV lower in energy; however, they found another isomer, containing two C_4 units, to be ~0.8 eV lower again. No evidence of Nb_4C_8 appears in our mass spectra, either because it is not made in great abundance in our source and/or its IP is greater than 5.91 eV.

D. Comparison with Analogous Clusters: Tantalum Carbide and Niobium Oxide Clusters. We have previously reported the IPs for the isovalent tantalum carbide clusters Ta_3C_n ($n = 1-3$) and Ta_4C_n ($n = 1-4$).[13] The IPs were assigned to those isomers where the C atoms attached to the Ta_m cluster in a manner to develop a $2 \times 2 \times 2$ nanocrystal. The extracted IPs for these species show trends that are very similar to the analogous niobium carbide clusters, although the IP reductions upon addition of C atoms are greater for the latter. However there are some differences to note. An IP onset was observed for Ta_3C but not for Nb_3C since it was beyond the range of our experiment (>5.91 eV). This is attributed to the fact that the in-plane structure (i.e., isomer A), is the global minimum for Nb_3C but has a much higher IP than the out-of-plane structure (i.e., isomer B). Conversely, the global minimum of Ta_3C is the out-of-plane structure. Additionally, IP onsets were not observed for Ta_3C_4, Ta_4C_5, and Ta_4C_6. It is not clear if these species are simply not generated under our experimental conditions or whether there are other factors at play. For example, it may be that for Ta_3C_4, the isomer with the low IP (i.e., VB) is not generated, while for Ta_4C_5 and Ta_4C_6 the higher spin states are not meta-stable. For all other Ta_mC_n species identified, the same structural isomers were assigned as the corresponding Nb_mC_n species.

The trends observed for the niobium carbide clusters are clearly different for those observed by Hackett and co-workers on the niobium oxide clusters.[17] Addition of one oxygen atom was observed to the niobium trimer, giving an IP reduction of −0.30 eV. For the tetramer, the IP is reduced upon addition of one oxygen atom (−0.11 eV) but is essentially unchanged upon addition of two oxygen atoms (−0.03 eV). The isomer of Nb_3C that we have assigned to the lower bound experimental IP has the same structure assigned to that of Nb_3O from a PFI-ZEKE study (i.e., a Nb−Nb edge bound atom).[7] Yet the former is calculated to substantially increase the IP, relative to Nb_3, while the latter decreases the IP. Clearly, the addition of carbon atoms to the niobium clusters changes the electronic properties quite differently to the addition of oxygen atoms.

It is also possible to look at the effect of individual O and C atoms on the IP of a metal cluster. The IPs of Nb_3CO and $Nb_3(CO)_2$ have been previously determined by us (and collaborators) to be 5.82 and 5.85 eV, respectively.[29] Comparison with DFT predictions and the lack of observed depletion in IR-MPD experiments suggest that the CO group(s) was dissociated in these clusters, i.e., the cluster contains separated C and O atoms. This appears to be consistent with the IP measurements. In comparison between Nb_3C_2 and Nb_3CO, the former substantially decreases the IP relative to Nb_3, while the IP of the latter is barely changed. From the calculated DFT geometries, Nb_3C_2 has the C atoms bound to the opposite Nb faces of the triangular Nb cluster. The bonding arrangements are quite different in Nb_3CO, where the C and O atom are bound across separate Nb−Nb edges. Again this demonstrates that carbon and oxygen atoms binding to niobium clusters affect not only the electronic structure quite differently but also the geometric structure.

E. Low-Lying Isomers and Meta Stable Electronic States. An interesting result of this study is the assignment of the observed ionization for Nb_3C_4, and possibly Nb_4C_6, to a structural isomer that is not the global minimum. As stated before, this does not imply that higher energy isomers are not present for other species in our experiment but rather that the threshold ionization technique favors the detection of isomers with the lower IP, with the caveat that they are present in sufficient concentration. If the onset of ionization is rapid (i.e., favorable FC overlap between the neutral and cationic states), it is unlikely that further ionization onsets due to other isomers will be discernible. Because of the uncertainty in the accuracy of the DFT calculations to predict the relative energies of isomers, it is entirely possible that any of the minima within 0.5 eV may be the global minimum. This is exemplified by the fact that even changing basis sets can lead to significant changes in relative energies, e.g., use of the extended basis set for the VA and VB isomers of Nb_3C_4 decreases the calculated energy difference from 0.679 to 0.183 eV, and for the XIIA and XIIE isomers of Nb_4C_6 increases the energy difference from 0.546 to 0.738 eV.

Under the conditions of a standard ablation source coupled to a condensation tube, where large number of collisions with the carrier gas occur, clusters attain thermal equilibrium (to room temperature in our case) in the *rotational* and *vibrational* degrees of freedom.[4,5] The IP values for several species (Nb_3, Nb_4 and Nb_3C_2) are slightly less (<0.05 eV) than those measured in previous studies that utilize a liquid nitrogen cooled source, which is consistent for clusters with a vibrational temperature of ~300 K.[7,8,16] Electronic cooling is somewhat different, and long-lived electronically excited states are well-known in several metal-containing systems.[30] However, this issue is deferred until later as it is the notion of *isomer* temperature that we wish to address first. This concept is well established from early microwave molecular beam studies of organic molecules where relative abundances of various isomers (or more correctly rotational conformers, which result from rotation of single bonds) with well-known energy differences can be controlled by varying the conditions (pressure, carrier gas, etc.) of the supersonic expansion.[31] One example is the rotation of the formyl group in propanal which produces two stable conformers with differing dihedral angles whose abundances can be controlled by changing the carrier gas and heating the source.[31–33] The concept of isomers is less established for metal clusters due to the difficulty in experimentally determining their geometric structures. About 15 years ago, several groups published work that showed the presence of at least two isomers for the clusters Nb_9-Nb_{12}, which exhibit different chemical reactivity (with D_2 and N_2) and different IPs.[16,34,35] For Nb_9, a biexponential fit to the reaction rate data revealed that the reactive isomer, R, is more abundant in the molecular beam than the unreactive isomer, U, by 25:1. The Nb_9 PIE curve showed an onset at 4.92 eV but following titration with D_2 (and hence removal of the *R* form), the PIE curve revealed the onset of the U form 0.28 eV higher in energy.[16] More recently, vibrationally induced dissociation spectroscopy experiments (or

IR-MPD) of Nb_9-Ar clusters similarly show the presence of two isomers, with different IR spectra, and a relative abundance of 1:0.3.[36] These workers also calculated DFT structures and energies for 3 isomers (A, B, and C) that had relative energies of 0.0, 0.15, and 0.82 eV, respectively, but only A and B correlated with the IR spectra. These two isomers, A and B, were then correlated with the previous IP and reactivity data, and it was concluded that B and A were the R and U isomers, respectively. Although both sets of data confirm that the B (or R) isomer is the more abundant in the various cluster sources, this isomer is calculated to be 0.15 eV higher than the global minimum energy structure.

On the basis of the preceding discussion, it therefore seems reasonable that in our experiments we have an isomer "temperature" in which we can consider two potentially observable isomers whose relative abundance may vary from 1:1 (i.e., degenerate in energy) to 1:10, assuming that a concentration of ~10% would be required for sufficient ion signal to be detected and that they have similar efficiencies for ionization. On the basis of this discussion it seems entirely reasonable that the Nb_3C_4, ionization is due to a low-lying isomer (VB, $\Delta E = +0.183$ eV). For Nb_4C_6, the calculated energy difference is 3−4 fold higher (XIIE, $\Delta E = +0.738$ eV) and the argument is less convincing; hence we prefer the assignment to a meta-stable state which is discussed now.

For Nb_4C_3 (the first, weak transition), Nb_4C_5, and also possibly for Nb_4C_6, we have assigned the onset of ionization to a transition that emanates from a long-lived, or meta-stable, electronic state. For all three systems, the ground-state is of singlet multiplicity and the proposed meta-stable state is a triplet, both of which can access the lowest-lying doublet state of the cation. In this sense, the assignment is plausible in that one could argue that any cluster species formed in the triplet state does not "collisionally cool" into the lower-energy singlet manifold due to a forbidden spin crossing. Such a meta-stable state would have to have a lifetime of at least several microseconds as well as survive approximately 10^4-10^5 collisions in the condensation tube before being supersonically cooled and isolated. Note that the situation is vastly different for the Nb_3C_n series where the potentially meta-stable (excited) quartet states cannot access the lowest energy singlet state of the cations. Thus, even if significant population is maintained in the quartet states, the observed transition will be to a triplet (or quintet) state, which we calculate (see Supporting Information) to be approximately the same energy as the doublet−singlet transition and hence will not be obvious in the PIE spectrum.

Long-lived excited electronic states have certainly been observed in small metal-containing systems isolated in supersonic expansions. The CoC radical has a $^2\Sigma^+$ ground state, as observed by laser induced fluorescence, but electronic transitions from an excited $^2\Delta_{5/2}$ state only 221 cm^{-1} higher in energy are also observed due to significant (meta-stable) abundance in the molecular beam.[30] Although it is well known that the density of states increases dramatically for dimers, trimers, and larger clusters, and therefore a higher probability of deactivating excited spin states,[37] Morse and co-workers have recorded jet-cooled spectra directly from meta-stable excited states of Ni_2 (an $\Omega = 4$ state calculated to be ~800 cm^{-1} higher than the $\Omega = 0$ ground state)[38] and Pt_2 (an unknown excited state, possibly $\Omega = 5$, that is calculated to be 614 cm^{-1} higher than the $\Omega = 0$ ground state).[39] For larger species, Scoles and co-workers recorded excitation spectra from meta-stable states of the Na_3 and K_3 alkali clusters formed in helium nanodroplets.[40] However, for larger transition metal clusters the authors are only aware of recent IR-MPD experiments using the FELIX free electron laser on the Nb_5^+-Ar and Nb_6-Ar clusters that show spectral features possibly arising from both singlet and triplet states, calculated to be only 0.16 and 0.01 eV different in energy, respectively.[41] In both cases, the observation of spectroscopic signatures from two spin multiplicities is indicative of significant population residing in the higher energy state, thus making them meta-stable on the time scale of the experiment. To sum up this discussion, in the case of Nb_4C_3, the assignment of the initial, weak ionization onset to a meta-stable triplet state, and not a higher energy isomer, we consider to be very strong. For Nb_4C_5 and Nb_4C_6, the assignment to a meta-stable state is the most plausible explanation, particularly given that both PIE curves are weak and flat, very similar to the first onset of Nb_4C_3. A more definite answer must await an exploration of the PIE curve to higher photon energies. Alternatively, IR-free electron laser experiments on these clusters may yield spectral data that can only be explained by significant molecular beam population of meta-stable excited states.

IV. Conclusions

We have recorded the ionization potentials for a series of Nb_3C_n ($n = 1-4$) and Nb_4C_n ($n = 1-6$) clusters and compared the values obtained with those calculated from DFT. For species where the number of carbon atoms is equal to, or less than, the number of niobium atoms, we find good correlation between the experimental IP and the relative IPs calculated for the lowest energy isomer calculated for each species, suggesting that the changes in electronic structure, and therefore geometric structure, which arise upon ionization, are correctly rationalized by theory. For Nb_3C_4 we find better correlation for a low-lying, higher energy isomer that contains a molecular C_2 unit. For Nb_4C_3, Nb_4C_5, and possibly Nb_4C_6, we propose the existence of meta-stable excited states that give rise to the observed ionization onsets; the latter two species contain one and two molecular C_2 units, respectively.

Acknowledgment. Financial support from the University of Adelaide's Faculty of Sciences is gratefully acknowledged. Support from the Australian Research Council for the purchase and maintenance of our lasers is also acknowledged. Computing resources provided by the Australian Partnership for Advanced Computing (APAC) and South Australian Partnership for Advanced Computing (SAPAC) is also gratefully acknowledged.

Supporting Information Available: A full list of calculated isomers at the SDD basis set and geometric parameters for the extended basis set isomers is provided in the Supporting Information file. This material is available free of charge via the Internet at http://pubs.acs.org.

References and Notes

(1) Duncan, M. A. *J. Cluster Sci.* **1997**, *8*, 239.
(2) Rohmer, M.-M.; Benard, M.; Poblet, J.-M. *Chem. Rev.* **2000**, *100*, 495.
(3) de Heer, W. A. *Rev. Mod. Phys.* **1993**, *65*, 611.
(4) Knickelbein, M. B. *Annu. Rev. Phys. Chem.* **1999**, *50*, 79.
(5) Simard, B.; Mitchell, S. A.; Rayner, D. M.; Yang, D.-S. *Metal-Ligand Interactions in Chemistry, Physics and Biology*; Russo, N., Salahub, D. R. Eds.; Kluwer Academic Publishers: Dordrecht, The Netherlands, 2000; pp 239.
(6) Pilgrim, J. S.; Brock, L. R.; Duncan, M. A. *J. Phys. Chem.* **1995**, *99*, 544.
(7) Yang, D.-S.; Hackett, P. A. *J. Electron Spectrosc. Relat. Phenom.* **2000**, *106*, 153.

(8) Yang, D.-S.; Zgierski, M. Z.; Berces, A.; Hackett, P. A.; Roy, P. N.; Martinez, A.; Carrington, T.; Salahub, D. R.; Fournier, R.; Pang, T.; Chen, C. *J. Chem. Phys.* **1996**, *105*, 10663.

(9) Brock, L. R.; Duncan, M. A. *J. Phys. Chem.* **1996**, *100*, 5654.

(10) van Heijnsbergen, D.; Fielicke, A.; Meijer, G.; von Helden, G. *Phys. Rev. Lett.* **2002**, *89*, 13401.

(11) von Helden, G.; van Heijnsbergen, D.; Meijer, G. *J. Phys. Chem. A* **2003**, *107*, 1671.

(12) Harris, H.; Dance, I. *J. Phys. Chem. A* **2001**, *105*, 3340.

(13) Dryza, V.; Addicoat, M. A.; Gascooke, J. R.; Buntine, M. A.; Metha, G. F. *J. Phys. Chem. A* **2005**, *189*, 11180.

(14) Frisch, M. J.; Trucks, G. W.; Schlegel, H. B.; Scuseria, G. E.; Robb, M. A.; Cheeseman, J. R.; Montgomery, J. A., Jr.; Vreven, T.; Kudin, K. N.; Burant, J. C.; Millam, J. M.; Iyengar, S. S.; Tomasi, J.; Barone, V.; Mennucci, B.; Cossi, M.; Scalmani, G.; Rega, N.; Petersson, G. A.; Nakatsuji, H.; Hada, M.; Ehara, M.; Toyota, K.; Fukuda, R.; Hasegawa, J.; Ishida, M.; Nakajima, T.; Honda, Y.; Kitao, O.; Nakai, H.; Klene, M.; Li, X.; Knox, J. E.; Hratchian, H. P.; Cross, J. B.; Bakken, V.; Adamo, C.; Jaramillo, J.; Gomperts, R.; Stratmann, R. E.; Yazyev, O.; Austin, A. J.; Cammi, R.; Pomelli, C.; Ochterski, J. W.; Ayala, P. Y.; Morokuma, K.; Voth, G. A.; Salvador, P.; Dannenberg, J. J.; Zakrzewski, V. G.; Dapprich, S.; Daniels, A. D.; Strain, M. C.; Farkas, O.; Malick, D. K.; Rabuck, A. D.; Raghavachari, K.; Foresman, J. B.; Ortiz, J. V.; Cui, Q.; Baboul, A. G.; Clifford, S.; Cioslowski, J.; Stefanov, B. B.; Liu, G.; Liashenko, A.; Piskorz, P.; Komaromi, I.; Martin, R. L.; Fox, D. J.; Keith, T.; Al-Laham, M. A.; Peng, C. Y.; Nanayakkara, A.; Challacombe, M.; Gill, P. M. W.; Johnson, B.; Chen, W.; Wong, M. W.; Gonzalez, C.; Pople, J. A. *Gaussian 03*, revision D.01; Gaussian, Inc.: Wallingford, CT, 2004.

(15) Glendening, E. D.; Reed, A. E.; Carpenter, J. E.; Weinhold, F. NBO Version 3.1.

(16) Knickelbein, M. B.; Yang, S. *J. Chem. Phys.* **1990**, *93*, 5760.

(17) Athanassenas, K.; Kreisle, D.; Collings, B. A.; Rayner, D. M.; Hackett, P. A. *Chem. Phys. Lett.* **1993**, *213*, 105.

(18) Fowler, J. E.; Garcia, A.; Ugalde, J. M. *Phys. Rev. A* **1999**, *60*, 3058.

(19) Majumdar, D.; Balasubramanian, K. *J. Chem. Phys.* **2001**, *115*, 886.

(20) Majumdar, D.; Balasubramanian, K. *J. Chem. Phys.* **2003**, *119*, 12866.

(21) Majumdar, D.; Balasubramanian, K. *J. Chem. Phys.* **2004**, *121*, 4014.

(22) Yeh, C. S.; Byun, Y. G.; Afzaal, S.; Kan, S. Z.; Lee, S.; Freiser, B. S.; Hay, P. J. *J. Am. Chem. Soc.* **1995**, *117*, 4042.

(23) Parnis, J. M.; Escobar-Caberra, E.; Thompson, M. G. K.; Jacular, J. P.; Lafleur, R. D.; Guevara-Garcia, A.; Martinez, A.; Rayner, D. M. *J. Phys. Chem. A* **2005**, *109*, 7046.

(24) Wang, H.; Craig, T.; Haouari, H.; Liu, Y.; Lombardi, J. R.; Lindsay, D. M. *J. Chem. Phys.* **1995**, *105*, 5355.

(25) Oshima, C.; Souda, R.; Aono, M.; Ontani, S.; Ishizawa, Y. *Phys. Rev. Lett.* **1986**, *56*, 240.

(26) Wang, L.-S.; Wang, X.-B.; Wu, H.; Cheng, H. *J. Am. Chem. Soc.* **1998**, *120*, 6556.

(27) Ge, M.; Feng, J.; Yang, C.; Li, Z.; Sun, C. *Int. J. Quantum Chem.* **1999**, *71*, 313.

(28) Munoz, J.; Rohmer, M.-M.; Benard, M.; Bo, C.; Poblet, J.-M. *J. Phys. Chem. A* **1999**, *103*, 4762.

(29) Pedersen, D. B.; Rayner, D. M.; Simard, B.; Addicoat, M. A.; Buntine, M. A.; Metha, G. F.; Fielicke, A. *J. Phys. Chem. A* **2004**, *108*, 964.

(30) Barnes, M.; Merer, A. J.; Metha, G. F. *J. Chem. Phys.* **1995**, *103*, 8360.

(31) Ruoff, R. S.; Klots, T. D.; Emilsson, T.; Gutowsky, H. S. *J. Chem. Phys.* **1990**, *86*, 3143.

(32) Randall, J.; Hardy, J. A.; Cox, A. P. *J. Chem. Soc., Faraday Trans. 2* **1988**, *84*, 1199.

(33) Metha, G. F.; Buntine, M. A.; McGilvery, D. C.; Morrison, R. J. S. *J. Mol. Spectrosc.* **1994**, *165*, 32.

(34) Bérces, A.; Hackett, P. A.; Lian, L.; Mitchell, S. A.; Rayner, D. M. *J. Chem. Phys.* **1998**, *108*, 5476.

(35) Hamrick, Y.; Taylor, S.; Lemire, G. W.; Fu, Z. W.; Shui, J. C.; Morse, M. D. *J. Chem. Phys.* **1988**, *88*, 4095.

(36) Fielicke, A.; Ratsch, C.; von Helden, G.; Meijer, G. *J. Chem. Phys.* **2005**, *122*, 091105.

(37) Morse, M. D. *Chem. Rev.* **1986**, *86*, 1049.

(38) Pinegar, J. C.; Langenberg, J. D.; Arrington, C. A.; Spain, E. M.; Morse, M. D. *J. Chem. Phys.* **1995**, *102*, 666.

(39) Fabbi, J. C.; Langenberg, J. D.; Costello, Q. D.; Morse, M. D.; Karlsson, L. *J. Chem. Phys.* **2001**, *115*, 7543.

(40) Reho, J. H.; Higgins, J.; Nooijen, M.; Lehmann, K. K.; Scoles, G.; Gutowski, M. *J. Chem. Phys.* **2001**, *115*, 10265.

(41) Fielicke, A.; Ratsch, C.; von Helden, G.; Meijer, G. *J. Chem. Phys.* **2007**, *127*, 234306.

JP800691S